Environmental Engineering and Management Journal

February 2015, Vol.14, No. 2, 399-408
http://omicron.ch.tuiasi.ro/EEMJ/

"Gheorghe Asachi" Technical University of Iasi, Romania

COPPER NANOPARTICLES SUPPORTED ON POLYETHER-FUNCTIONALIZED MESOPOROUS SILICA. SYNTHESIS AND APPLICATION AS HYDROGENATION CATALYSTS

Constantin Rudolf[1], Irina Mazilu[1], Alexandru Chirieac[1], Brandusa Dragoi[1], Fatima Abi-Ghaida[2], Adrian Ungureanu[1], Ahmad Mehdi[2], Emil Dumitriu[1*]

[1] *"Gheorghe Asachi" Technical University of Iasi, Faculty of Chemical Engineering and Environmental Protection, Laboratory of Catalysis, 73 Prof. Dr. docent Dimitrie Mangeron Str., 700050 Iasi, Romania*
[2] *University of Montpellier, The Institute Charles Gerhardt of Montpellier, UMR 5253, Molecular Chemistry and Solid Organisation, cc 1701, Place E. Bataillon, 34095 Montpellier, Cedex 5 France*

Abstract

Copper nanoparticles were successfully synthesized on polyether-functionalized mesoporous silica to investigate the effect of metal loading (10, 25 and 35 wt. % Cu) on their structural and catalytic properties. The oxide forms of these nanocomposite materials were thoroughly characterized by nitrogen physisorption, SAXS, WAXS, TEM, EDXS, and TPR, whereas the metallic forms were analysed by N_2O chemisorption. The results indicated that the mesostructured SBA-15-like hybrids favoured the generation of highly dispersed supported copper nanoparticles with average sizes in the range of ~2-6 nm, displaying excellent activity in the hydrogenation of cinnamaldehyde. The average particle size was shown to increase with the metal loading. Among the tested catalysts, the highest activity was obtained for the sample having 25 wt. % Cu (total conversion of cinnamaldehyde in 150 min of reaction). All the catalysts exhibited high selectivity towards hydrocinnamaldehyde (> 85 mol %), which did not appear dependent on the copper particle size.

Key words: Cu-based catalysts, hydrogenation of cinnamaldehyde, polyether-functionalized mesoporous materials

Received: November, 2014; Revised final: February, 2015; Accepted: February, 2015

1. Introduction

The unique electronic structure and the high active surface of metal (oxide) nanoparticles (NPs) have motivated extensive researches focused on developing new performing heterogeneous catalysts with potential applications in fine chemistry, petrochemistry, pollution prevention (Jansat et al., 2007) and other important fields (Campelo et al., 2009). For such applications, the most common type of catalysts comprises metal (oxide) NPs deposited on inorganic or organic porous supports, which provide high-surface areas and specific local environments to stabilize highly dispersed catalytic active phases. It was reported that the main features that influence the activity, selectivity, and lifetime of such supported nanocatalysts are the particle structure and morphology (size and shape), their chemical composition and the oxidation state, which in turn, are dependent on many factors such as the nature of metal/catalytic precursor, the nature of the support and the interactions between the metal and support, all of which are in close connection with the preparation method (Cuenya, 2010).

Extensive efforts have been made to control the structure and morphology of NPs on supported catalysts, but the development of a simple strategy for the preparation of highly dispersed metal (oxide) particles remains a challenge, particularly in the case of copper-based catalysts. For instance, it was shown

* Author to whom all correspondence should be addressed: e-mail: edumitri@tuiasi.ro

that bulk copper catalysts are not active in hydrogenation reactions, but reduction in the particle size of metallic copper (up to 10 nm or smaller) changes its electronic structure, the number of defects on the crystal surface, and the distribution of surface sites, thus leading to enhanced catalytic activity (Dragoi et al., 2010; Mäki-Arvela et al., 2005; Ungureanu et al., 2013). It is also known that Cu clusters do not chemisorb H_2 molecules because they need to pass an activation barrier (Andersson et al., 1996; Morse et al., 1985), which could be easily overpassed by small crystals, as also predicted by theoretical calculations (Guvelioglu et al., 2006; Yang et al., 2010).

Therefore, many attempts were reported to control the size and the shape of copper NPs, which to date remains a very challenging goal because of the high mobility of copper ions resulting in significant sintering (even at low temperatures) and formation of large aggregates (Munnik et al., 2011). Furthermore, such lack of control substantially magnifies with increasing copper loading.

In order to achieve high dispersion and stability of copper NPs supported on inorganic supports, various strategies were applied. These include controlled calcination conditions (Munnik et al., 2011), drying at ambient temperature (Toupance et al., 2000), incipient wetness impregnation followed by mild drying (IWI-MD) (Ungureanu et al., 2013) or vacuum–thermal treatment (Liu et al., 2014), the promoting effect caused by a second metal (Dragoi et al., 2013; Ungureanu et al., 2013), mild reduction of Cu^{2+} substituted in a LDH matrix (Chirieac et al., 2012; Dragoi et al., 2011) etc. Nonetheless, the experimental results indicated that the stability of Cu-NPs is far from being resolved, especially at high metal loading. Simultaneously, the most significant strategy is based on the preparation of catalysts by impregnation on silica supports. In the case of incipient wetness impregnation, the water volume used for metal precursors is lower than the pore volume of the support.

Hence, it is often difficult to prepare catalysts with high degrees of metal loading due to the limited amount of solvent. This drawback can be easily overcome by applying the solvent-free melt infiltration method (MI) (de Jongh and Eggenhuisen, 2013). This emergent synthetic methodology not only provides an alternative to the classical wet preparation approaches, but it also facilitates extended control over the spatial distribution of NPs throughout the porosity of support, notably because the drying step to remove solvents is absent, which is known to bring about the redistribution of precursor species and formation of undesired bulky agglomerates. Furthermore, melt infiltration can be successfully applied on as-synthetized mesostructured supports, providing a very significant example on how the microenvironment existing between polymeric fragments and inorganic walls can be rationally explored to include high amounts of metal precursors and generate highly dispersed metal (oxide) nanoparticles (Tian et al., 2010; Yin et al., 2012).

Therefore, this study is aimed at successfully preparing catalysts with different contents of copper (from 10 up to 35 wt. % Cu) deposited on a functional SBA-15-like mesoporous silica support by using IWI-MD and MI methods followed by investigating the influence of metal loading on the particle size of metallic copper and its impact on the catalytic performances. Mesoporous materials with SBA-15 topology were previously shown to exhibit excellent properties as catalytic supports for metal (oxide) NPs owing to the large specific surface areas and well defined pore structures (Munnik et al., 2011; Sietsma et al., 2008).

Moreover, these materials are prone to one-pot or post-synthetic functionalization with various organic groups, resulting in functional inorganic-organic hybrid mesostructures. Such functionalization offers specific tailoring of the surface chemical properties which improves the interaction between metal precursors and pore surfaces thus leading to high dispersions of copper NPs stabilized within the pores (Athens et al., 2009). For instance, Cu-NPs with 2−6 nm in average size and metal loadings of 7.6−25.2 wt. % can be successfully prepared by immobilization on hybrid SBA-15 supports functionalized with carboxylic acid groups (Chen et al., 2013). Herein, we utilized a different strategy to deposit highly dispersed copper NPs on SBA-15-like mesoporous silica. A functionalized bis-silylated triblock copolymer Pluronic P123 containing triethoxysilyl moieties at the chain ends was prepared, according to a procedure previously reported (Grandsire et al., 2010).

The functionalized Pluronic P123 acted thereafter as both a structure direction agent (SDA) for the two-dimensional hexagonal SBA-15-like mesostructure containing the original polyether groups of the surfactant covalently bound to the silica framework and a dispersing agent for the copper precursors to be subsequently impregnated/infiltrated into the support porosity, respectively. As a novel hybrid SBA-15-like support material, this polyether-functionalized mesoporous silica presented enhanced capacity to stabilize Cu NPs having outstanding catalytic performances in cinnamaldehyde hydrogenation. This reaction is very interesting from a fundamental point of view (control of the chemoselectivity) and it has been largely investigated (Mäki-Arvela et al., 2005). Also, it is of industrial relevance since the products of partial and total hydrogenation are being used in flavour and perfume industry, cosmetics etc.

It is worthy to note that a wide variety of efficient noble metal-based catalysts were reported for the hydrogenation of cinnamaldehyde, amongst which are platinum (Chatterjee et al., 2004; Jung et al., 2009; Li et al., 2008; Richard et al., 1989; Rylander, 1967; Samant et al., 2005), iridium (Giroir-Fendler et al., 1988; López-Linares et al., 1999),

ruthenium (Hájek et al., 2003; Liu et al., 2011; Toebes et al., 2003), and rhodium (Reyes et al., 2000). Albeit their great potential to replace the expensive noble metal-base catalysts, the cost-effective copper-based catalysts were barely reported in cinnamaldehyde hydrogenation (Gutiérrez et al., 2011, 2012).

2. Experimental

2.1. Bis-silylated P123 synthesis

Bis-silylated P123 (Si-P123) was synthesized according to Grandsire et al., 2010 as follows: a solution of 10 g (1.72 mmol) of Pluronic P123 (poly(ethyleneoxide)-block-poly(propyleneoxide)-block-poly(ethyleneoxide)-block), $EO_{20}PO_{70}EO_{20}$, molecular weight of 5800, BASF Corp.) in CH_2Cl_2 (200 mL) was dried with magnesium sulfate and filtered. CH_2Cl_2 was removed and polymer was heated under vacuum at 100 °C for 12 h. Dry P123 was then silylated with 3-isocyanatopropyltriethoxysilane (ICPTES). To a solution of P123 (0.1 M) in dry THF (100 mL), an excess of ICPTES (4 equiv.) and Et_3N (2 equiv.) were added at room temperature. The mixture was stirred at reflux for 72 h under argon. After removal of THF and Et_3N, the obtained crude was washed with pentane four times and dried, giving rise to 9.39 g (1.50 mmol, 87%) of Si-P123 as colourless oil.

2.2. Supports and catalysts preparation

The polyether-functionalized mesoporous silica support was obtained according to the previously reported method (Grandsire et al., 2010). Thus, for 5.6 g of powder, in an Erlenmeyer flask, an amount of 8.6 g (1.36 mmol) of Si-P123 as SDA was solubilized in 300 mL of an aqueous HCl solution having a pH of 1.5. After 2-3 h of stirring, the solution was poured into another flask containing 18.7 g (89.78 mmol) of tetraethylorthosilicate ($Si(OC_2H_5)_4$, TEOS) at room temperature.

The reaction mixture was left for 2 h and 30 min. at room temperature under vivid and regular magnetic stirring to give rise to a microemulsion: the solution is perfectly clear and colourless. The flask was immersed in an oil bath at 60 °C then (after 2 minutes) 150 mg (3.6 mmol) of NaF was added under stirring to allow hydrolysis-polycondensation. A white precipitate formed within few minutes. The reaction mixture was left under stirring for 72 hours at 60 ° C, the resulting powder was filtered off and the unbound surfactant was removed by Soxhlet extraction over ethanol for 24 hours and finally dried at 120 °C under vacuum. The polyether-functionalized mesoporous silica was denoted as M100, where *"*M*"* stands for mesoporous support and "100" stands for the molar ratio of bis-silylated P123 used in synthesis (no P123 was used). According to thermogravimetric analysis, the organic fraction in dried M100 material was of ~25 wt. % (weight loss up to 500 °C under air).

Metal oxide-loaded mesoporous support with 10 wt.% zero-valent metal loading was prepared by incipient wetness impregnation, followed by mild drying (IWI-MD) (Ungureanu et al., 2013). A certain amount of M100 support was placed in contact with the corresponding aqueous copper nitrate precursor solution. The metal precursor/hybrid SBA-15 composites were gently dried under air at 25 ± 1 °C for 5 days. The powders were sequentially submitted to calcination under stagnant air in a muffle oven at 500 °C for 6 h (heating ramp of 1.5 °C·min^{-1}) to obtain the oxide forms of catalysts and burn off the organic components. The sample was denoted as Cu_{10}/M100.

To study the effect of metal loading, two samples with 25 and 35 wt. % Cu, respectively were prepared by an optimized melt infiltration (MI) procedure. Basically, the method consists of mixing the appropriate amounts of $Cu(NO_3)_2{\cdot}3H_2O$ and hybrid support, followed by continuous grinding for 45 minutes. The solid mixture was transferred to a Teflon autoclave and subjected to a heat treatment at 120 ° C for several days, followed by cooling down to room temperature. The obtained infiltrates were calcined under the same conditions as above. These samples were denoted as Cu_{25}/M100 and Cu_{35}/M100, according to their metal loading.

A mesoporous alumina sample (denoted as MA) was also synthesized via Evaporation-Induced Self-Assembly (EISA) technique by using P123 as SDA (according to Yuan et al., 2008) and used as support. CuO-loaded mesoporous alumina (10 wt. % Cu) was also prepared by MI (sample Cu_{10}/MA) and used as reference.

2.3. Catalyst characterization

Nitrogen physisorption was carried out at −196 °C on an Autosorb 1-MP instrument from Quantachrome. Surface areas and pore volumes were calculated from the corresponding isotherms using conventional algorithms.

Temperature programmed reduction (TPR) and chemisorption experiments were performed on a Chembet Pulsar TPR/TPD from Quantachrome. About 30 mg of calcined sample were inserted in a U-shape microreactor. Before each TPR run, the catalyst was activated at 500 °C for 1 h under a flow of simulated air (40 mL min−1). After cooling to 50 °C, the H_2 containing flow was stabilized (40 mL min^{-1}, 5 vol. % H_2 in Ar) and the TPR was performed from 50 to 500 °C with a temperature ramp of 5 °C min^{-1}.

The dispersion of metallic copper (D_{Cu}), average copper particle size (d_{Cu}) and active surface area (S_{Cu}) were determined using a nitrous oxide chemisorption method using specific algorithms (Chinchen et al., 1987; Evans et al., 1983; Jun et al., 1998; Krishna et al., 1999). The experiments were conducted in a quartz U-tube reactor, where an

amount of about 30 mg of the sample was introduced and fixed with quartz wool. The first reduction was carried out under the same conditions used for TPR, up to 500 °C. After the reduction step, the gas was switched to Ar and the reactor was cooled down to 50 °C, kept for 30 min., and then the gas was switched to N_2O (40 mL min^{-1}) for 30 min. in order to oxidize the surface zero-valent Cu to Cu_2O. The sample was again flushed with pure Ar for 30 min., and then a second TPR run was performed.

Energy X-Ray dispersive spectroscopy (EDXS) analyses were performed with an environmental scanning electronic microscope Quanta 200 coupled with an Oxford INCA analyzer. The Transmission Electron Microscopy (TEM) observations were carried out at 100 kV on a JEOL 1200 EXII microscope at the Service Commun de Microscopie Electronique (UM2, Montpellier, France). The SAXS and WAXS experiments were made on ID02 at 12.4keV with d=1.5m. The samples were inserted between two Kapton glasses. All measurements were dark subtracted and the background was measured with a double empty Kapton glass. All measurements were normalized by the transmission coefficient and by the acquisition time.

2.4. Catalytic activity

The catalytic liquid phase hydrogenation of cinnamaldehyde was carried out at atmospheric pressure in a round-bottom three-necked glass reactor equipped with a bubbler, a magnetic stirrer and a reflux condenser. The following reaction conditions were applied: 0.265 g of catalyst, 1.0 mL of trans-cinnamaldehyde, 25.0 mL of propylene carbonate as solvent, hydrogen flow of 1.0 $L.h^{-1}$, reaction temperature of 150 °C, and stirring speed of 900 rpm. At certain periods, aliquots of reaction mixture were withdrawn and analyzed with a gas-chromatograph (HP 5890 equipped with a DB-5 capillary column (25 m × 0.20 mm × 0.33 μm) and FID detector).

The products were identified from the retention time of the pure compounds and also verified with a GC-MS (Agilent 6890N system equipped with an Agilent 5973 MSD detector and a DB-5-ms column). For the quantitative analyses, the FID response factors for each compound were taken into consideration. The selectivity towards the products and the total conversion were calculated in a previous paper. (Dragoi et al., 2010)

3. Results and discussion

3.1. Structural and textural properties

The textural characteristics of the metal oxide-loaded samples were evaluated from the nitrogen adsorption–desorption isotherms (Fig. 1) and compared with those of the calcined M100. All materials display isotherms of type IV with hysteresis loops of type H1. The isotherms of both, the metal oxide samples and the calcined samples are characteristic of ordered SBA-15-like mesostructures having narrow size distributions of the cylindrical mesopores, indicating that the mesoporous structure of the support was retained after the deposition of copper oxide.

However, with the gradual rise in metal loading, a continuous decrease in the nitrogen uptake at high relative pressure can be observed, suggesting a corresponding reduction in pore volume, which can be associated with the successful deposition of more copper oxide NPs within the porosity of the support. Moreover, no forced closures of the hysteresis loops are observed on the desorption branches of the isotherms, suggesting the absence of cavitation effects resulting from the partial blockage of primary mesopores with metal oxide NPs, which usually occurs when all particles are confined whitin the main mesopores of the support (Ungureanu et al., 2013).

The pore size distribution curves shown in Fig. 2 are in good agreement with the adsorption/desorption isotherms. Thus, all solids have narrow pore size distribution of the main channels (Kruk and Jaroniec, 2001) when compared with the calcined M100 (curve a) where the maxima of the differential pore volume for Cu_{10}/M100 and Cu_{25}/M100 (curves b and c) are slightly shifted to lower values (9.2 *vs* 9.6 nm), whereas for Cu_{35}/M100 (curve d) the maximum was found to be essentially unchanged (9.8 *vs* 9.6 nm) owing to the different dispersion degrees of CuO NPs and different particle size distribution as a function of metal loading.

The evaluation of the textural properties of the calcined samples based on the nitrogen adsorption/desorption isotherms reveals a progressive decrease in the specific surface area as a function of the metal loading, from 943 m^2/g (M100) to 437 m^2/g (Cu_{35}/M100), in parallel with a decrease in the total pore volume, from 1.52 to 0.71 cm^3/g (Table 1).

Likewise, the micropore surface area steadily falls from 301 m^2/g (M100) to 126 m^2/g (Cu_{25}/M100). Further increase in the copper loading (35 wt. %) maintains a nearly constant surface area (121 m^2/g). It is therefore likely that a population of CuO crystallites had suffered the nucleation and growth inside/at the mouth of the microporous domains generating stable micropore-encapsulated oxide NPs, whose fraction seems to be maximum at a metal loading of 25 wt. %.

Fig. 3 shows the SAXS results obtained for the calcined Cu/M100 materials with different metal loadings. For all samples, the patterns display very intense peaks indexed to the (100) planes and two less intense peaks indexed to the (110) and (200) planes of highly ordered hexagonal 2D structures with *p6mm* symmetry (Boubekr et al., 2011; Imperor-Clerc et al., 2004), confirming thus the physisorption results. No significant shifts of the *q* values with the increase in metal loading were observed, indicating similar unit cell parameters of the obtained mesostructured composites.

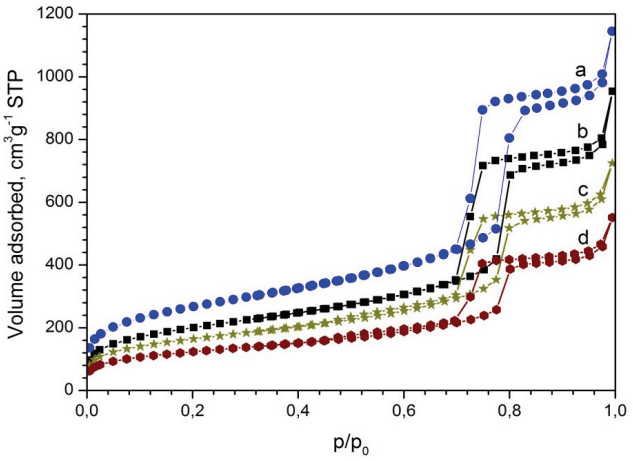

Fig. 1. N_2 physisorption isotherms for calcined a) M100, b) Cu_{10}/M100, c) Cu_{25}/M100 and d) Cu_{35}/M100

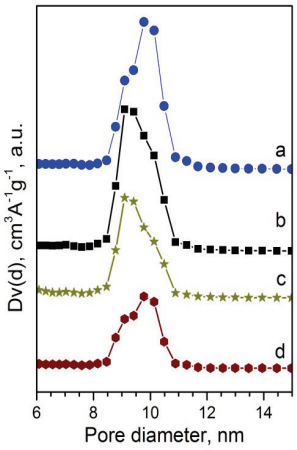

Fig. 2. NL-DFT pore size distributions for calcined a) M100, b) Cu_{10}/M100, c) Cu_{25}/M100 and d) Cu_{35}/M100

Table 1. Textural properties of calcined Cu/M100 materials

Sample	S_{BET} (m^2/g)	D_p *(nm)*	V_p (cm^3/g)	S_μ (m^2/g)	V_μ (cm^3/g)
M100	943	9.6	1.52	301	0.14
Cu_{10}/M100	714	9.2	0.98	188	0.08
Cu_{25}/M100	577	9.2	0.95	126	0.06
Cu_{35}/M100	437	9.8	0.71	121	0.05

S_{BET} – specific surface area, D_p – mean mesopore diameter, V_p – total pore volume, S_μ – micropore surface area, V_μ – micropore volume

Simultaneously, the relative intensities of the different peaks seem to be unaltered, which is in agreement with the retention of the mesostructural ordering of the support after the deposition of CuO NPs. However, a clear decrease in the overall intensity occurs with the increase in the loading from 10 to 25 wt.% (patterns a and b), note that the intensity does not change at higher loading of 35 wt.% (pattern c).

Since the intensity of the (100) peak is directly proportional to the square of the electron density difference between the silica walls and the oxide phase located inside the pores (Imperor-Clerc et al., 2004), the less intense peaks observed herein at loadings of 25 and 35 wt. % suggests that the extent of filling of the main mesopores with CuO-NPs is higher than those corresponding to 10 wt. %.

The results can be readily explained by taking into account the tendency of copper precursors to aggregate, especially at high loadings, either within the main mesopores forming confined oxidic aggregates or at the external surface of support grains giving rise to bulky oxide particles (Munnik et al., 2011). Indeed, the WAXS patterns of Cu_{25}/M100 and Cu_{35}/M100 solids (Fig. 4, patterns b and c) exhibit diffraction peaks characteristic to monoclinic CuO, whose intensity follows the metal loading of the catalysts.

However, introspection on these two patterns discloses that the diffraction peaks are asymmetric in shape and with obvious broadened onsets, signifying that two populations of CuO crystallites must be present in these composites: *(i)* intra-porous, highly dispersed CuO-NPs, which are likely confined in the micropores and/or main mesopores and *(ii)* extra-porous CuO large aggregates. In contrast, Cu_{10}/M100 sample displays hardly distinguishable CuO diffraction peaks, clearly indicating the presence of only nanosized oxidic crystallites.

Transmission electron microscopy (TEM) images recorded at low-resolution for the copper-based nanocomposites are presented in Fig. 5. As a first observation, both solids exhibit typical highly-ordered mesoporous SBA-15-like structures composed of cylindrical mesochannels with narrow size distribution, in line with SAXS and N_2 physisorption results. No large aggregates on the external surface of silica grains were observed for the sample Cu_{10}/M100 (image a). In contrast, extra-porous large particles (as indicated by an arrow in image b) appeared for the sample Cu_{35}/M100. These observations confirm that as the copper loading increases from 10 wt. % to higher loadings, the distribution of particles sizes becomes more heterogeneous, in good agreement with WAXS. Nevertheless, the highly dispersed intra-porous copper particles cannot be clearly distinguished in the corresponding TEM images.

3.2. Reducible properties and copper dispersion

The EDXS results confirm that the metal loading degrees are close to the calculated ones (Table 2). The reducibility of CuO-loaded materials was analysed by TPR and the results are illustrated in Fig. 6.

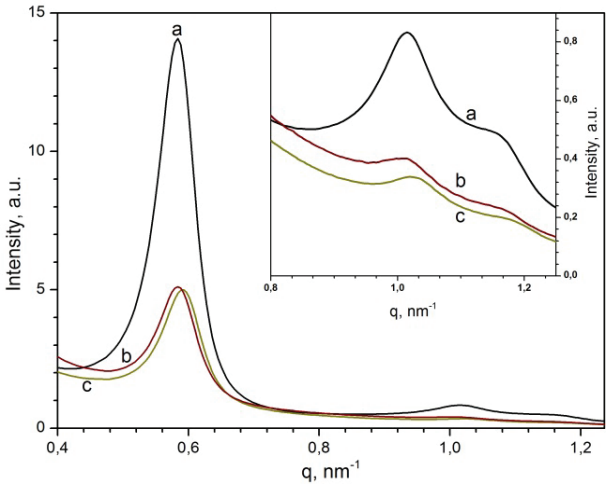

Fig. 3. SAXS patterns for a) Cu_{10}/M100, b) Cu_{25}/M100 and c) Cu_{35}/M100

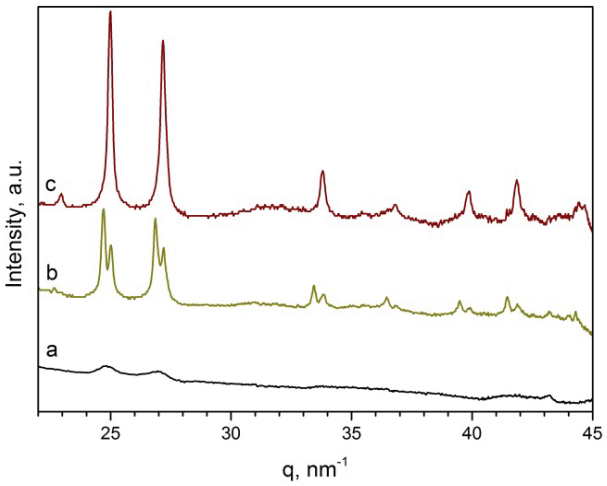

Fig. 4. WAXS patterns for a) Cu_{10}/M100, b) Cu_{25}/M100 and c) Cu_{35}/M100

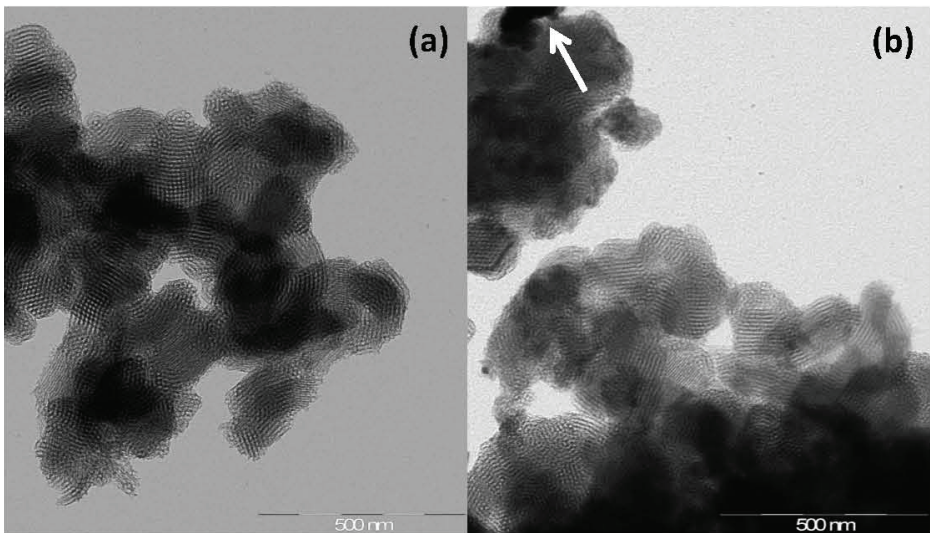

Fig. 5. Low-resolution TEM images for a) Cu_{10}/M100 and b) Cu_{35}/M100

Table 2. EDXS and N_2O chemisorption results

Sample	***EDXS Cu (wt. %)***	***N_2O chemisorption***			
		D_{Cu} (%)	***d_{Cu} (nm)***	***S_{Cu} (m^2/g_{Cu})***	***S_{Cu} (m^2/g_{cat})***
Cu_{10}/M100	12.6	43.5	2.3	294.3	37.1
Cu_{25}/M100	23.6	25.1	4.0	169.8	40.1
Cu_{35}/M100	33.8	16.7	6.0	113.0	38.2
Cu_{10}/MA	10.5	9.0	11.0	60.9	6.4

D_{Cu} - dispersion degree, d_{Cu} – average size of Cu particles, S_{Cu} – Cu surface area

As a first observation, the experimental hydrogen consumption was in good agreement with the theoretical consumption calculated by elemental analysis of the calcined samples, which indicates that the presented TPR profiles reflect the complete reduction of CuO to zero-valent metallic Cu.

The TPR profile for Cu_{10}/M100 (curve b) displays a single step reduction at ~270 °C, which indicates a homogenous distribution of the highly dispersed CuO particles. In contrast, Cu_{25}/M100 and Cu_{35}/M100 samples show two-step reduction profiles, which are characterized by main peaks at ~300 °C and shoulders at ~270 °C. According to literature, the reduction temperature of CuO depends on the particle size and dispersion, lower temperatures being usually associated to higher dispersion (Tu et al., 2006; Zheng et al., 2005). Under these considerations, TPR results for the samples with high metal loadings indicate a heterogeneous distribution of CuO particles sizes, in agreement with TEM: the main peaks are attributed to weakly dispersed CuO probably under the form of extra-porous aggregates whereas the shoulders are due to the highly dispersed intra-porous CuO

particles. On the other hand, Cu_{10}/MA reference material displays a reduction maximum at ~290 °C, pointing out a much lower CuO dispersion, as compared with the copper material obtained on the mesostructured SBA-15-like hybrid.

To evaluate copper dispersion, the titration of superficial copper atoms with N_2O was performed. Table 2 centralizes the dispersion degrees, Cu surface areas, and Cu average particle sizes for all catalysts. Cu/M100 catalysts showed high dispersion degrees that fall from 43.5 to 25.1 and 16.7 % by increasing the metal loading from 10 to 25 and 35 wt.%, respectively.

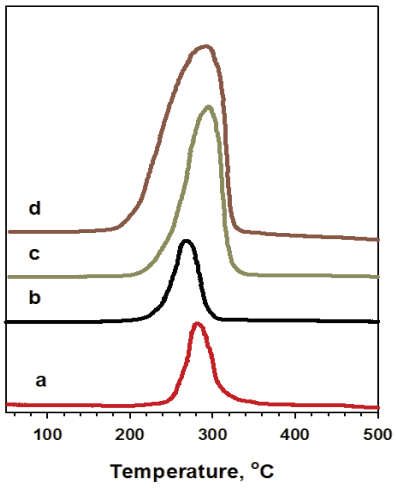

Fig. 6. TPR profiles for Cu_{10}/MA (a), Cu_{10}/M100 (b), Cu_{25}/M100 (c), and Cu_{35}/M100 (d)

In parallel, the estimated values of Cu particle size range between 2.3 and 6.0 nm, indicating that small metallic copper NPs are generated by the reduction of highly dispersed CuO-NPs, as already demonstrated by various techniques. As awaited, the average particle size increases with the copper loading, whereas the active surface per gram of copper decreases. It is however interesting to observe that Cu surface area per gram of catalyst shows a maximum value of 40.1 m^2/g for the Cu_{25}/M100 sample, which is thus expected to show the highest catalytic activity. It is also worthy to note that a similar high value of Cu surface area (45.8 m^2/g) was previously reported for 25.2% Cu/SBA-15 prepared by impregnation on hybrid SBA-15 functionalized with carboxylic acid groups (Chen et al., 2013), as a confirmation on the high capacity of our approach to stabilize highly dispersed Cu NPs even at high loading degree. On the other hand, as expected, Cu_{10}/MA showed a much lower dispersion (9 %) and larger particle size (11 nm) as compared with Cu_{10}/M100.

3.3. Catalytic properties

The obtained materials were finally tested in the catalytic hydrogenation of trans-cinnamaldehyde (Fig. 7) with the purpose of investigating the activity and selectivity in relation with the metal loading degree. The evolution of CNA conversion *vs* time is presented in Fig. 8. It can be observed that all catalysts obtained on M100 supports are highly active in hydrogenation where complete conversion of the substrate takes place in a maximum of 240 min. of reaction duration.

The results are very interesting while considering the mild reaction conditions, especially the atmospheric pressure. Under the same conditions, Cu_{10}/MA displays a poor activity, which can be readily connected with the lowest dispersion and Cu surface area (see Table 2). Although all Cu/M100 materials were very active, the conversion curves shown in Fig. 8 indicate that the catalytic activity follows the order: Cu_{25}/M100 > Cu_{10}/M100 ~ Cu_{35}/M100, these are in good agreement with the evolution of S_{Cu} (m^2/g_{cat}) (Table 2), Cu_{25}/M100 sample displaying the highest active surface of 40.1 m^2/g. The results clearly demonstrate that a loading of 25 wt. % Cu is optimum to achieve high activity correlated with the highest number of active sites. Regarding the selectivity, as shown in Table 3, it can be concluded that Cu/M100 catalysts are highly selective towards the saturated aldehyde (more than 85 mol % HCNA).

Furthermore, the selectivity profiles were almost identical for all catalysts, suggesting that the chemoselectivity does not depend on the copper particle size, as far as the range of 2.3-6 nm is considered.

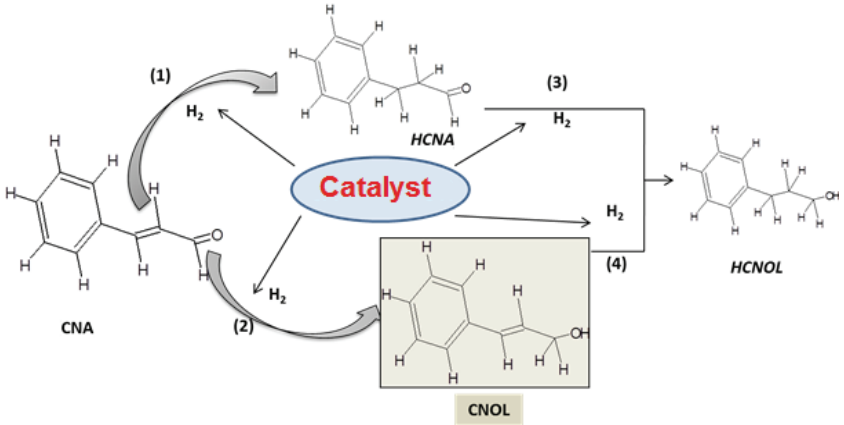

Fig. 7. Reaction pathways for the hydrogenation of cinnamaldehyde

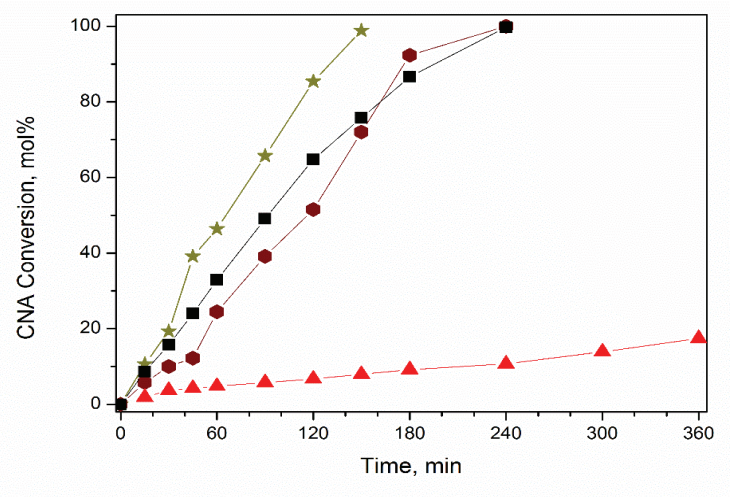

Fig. 8. Catalytic activity of copper NPs supported on M100
■-Cu_{10}/M100, ★-Cu_{25}/M100, ⬢-Cu_{35}/M100,▲-Cu_{10}/MA

Table 3. Selectivity of copper NPs supported on M100

Sample	***Selectivity* (mol %)***		
	HCNA	***CNOL***	***HCNOL***
Cu_{10}/M_{100}	86.5	3.5	10.0
Cu_{25}/M_{100}	85.9	1.7	12.4
Cu_{35}/M_{100}	88.5	4.6	6.9

**selectivity measured after 120 min*

4. Conclusions

Bis-silylated mesoporous silica was successfully loaded with large amounts of copper, up to 35 wt. %, while maintaining good dispersion degrees and very high copper active surfaces. Nevertheless, metal loadings higher than 10 wt. % resulted in lower dispersions of CuO-NPs, which appear heterogeneously distributed on the mesoporous silica support as both large agglomerates and highly dispersed particles, respectively.

As a consequence, the average particle size of metallic copper increased with the metal loading from 2.3 to 6 nm. The catalysts manifested excellent activity in the hydrogenation of cinnamaldehyde, with a maximum for the sample with 25 wt. % Cu, and high selectivity towards hydrocinnamaldehyde (> 85 mol %), which however did not depend on the copper particle size.

Due to these interesting results, bis-silylated mesoporous hybrid materials with different contents in the functionalized P123 were designed and used for detailed investigations on the effect of surface microenvironment on copper particle structure and morphology, which will constitute the subject of a distinct contribution.

Acknowledgments

This work was partially supported by two grants of the Romanian National Authority for Scientific Research, CNCS-UEFISCDI (project numbers PN-II-RU-TE-2012-3-0403 and PN-II-CT-RO-FR-2012-1-0052 - Bilateral program Hubert Curien-Brancusi).

References

Andersson M., Persson J.L., Rosén A., (1996), Reactivity of Fe_n, Co_n, and Cu_n clusters with O_2 and D_2 studied at single-collision conditions, *The Journal of Physical Chemistry,* **100**, 12222-12234.

Athens G.L., Shayib R.M., Chmelka B.F., (2009), Functionalization of mesostructured inorganic–organic and porous inorganic materials, *Current Opinion in Colloid & Interface Science*, **14**, 281-292.

Boubekr F., Davidson A., Casale S., Massiani P., (2011), Ex-nitrate Co/SBA-15 catalysts prepared with calibrated silica grains: Information given by TPR, TEM, SAXS and WAXS, *Microporous and Mesoporous Materials*, **141**, 157-166.

Campelo J.M., Luna D., Luque R., Marinas J.M., Romero A.A., (2009), Sustainable preparation of supported metal nanoparticles and their applications in catalysis, *ChemSusChem*, **2**, 18-45.

Chatterjee M., Zhao F.Y., Ikushima Y., (2004), Effect of synthesis variables on the hydrogenation of cinnamaldehyde over Pt-MCM-48 in supercritical CO_2 medium, *Applied Catalysis A: General,* **262**, 93-100.

Chen C.S., Lai Y.T., Lai T.W., Wu J.H., Chen C.H., Lee J.F., Kao H.M., (2013), Formation of Cu nanoparticles in SBA-15 functionalized with carboxylic acid groups and their application in the water−gas shift reaction, *ACS Catalysis*, **3**, 667-677.

Chinchen G.C., Hay C.M., Vandervell H.D., Waugh K.C., (1987), The measurement of copper surface areas by reactive frontal chromatography, *Journal of Catalysis,* **103**, 79-86.

Cuenya B.R., (2010), Synthesis and catalytic properties of metal nanoparticles: size, shape, support, composition, and oxidation state effects, *Thin Solid Films*, **518**, 3127-3150.

de Jongh P.E., Eggenhuisen P., (2013), Melt infiltration: an emerging technique for the preparation of novel functional nanostructured materials, *Advanced Materials,* **25**, 6672-6690.

Dragoi B., Ungureanu A., Chirieac A., Hulea V., Dumitriu E., (2010), Hydrogenation of unsaturated carbonyl compounds on non-calcined LDHs. I. Synthesis and characterization of ZnNiCuAl hydrotalcite-like materials, *Acta Chimica Slovenica,* **57**, 677-685.

Dragoi B., Ungureanu A., Chirieac A., Dumitriu E., (2011), Synthesis of new catalysts by insertion of Co and Cu in the matrix of hydrotalcite-like materials for cinnamaldehyde hydrogenation, *Environmental Engineering and Management Journal,* **10**, 1561-1571.

Dragoi B., Ungureanu A., Chirieac A., Hulea V., Royer S., Dumitriu E., (2013), Enhancing the performance of SBA-15-supported copper catalysts by chromium addition for the chemoselective hydrogenation of trans-cinnamaldehyde, *Catalysis Science and Technology,* **3**, 2319-2329.

Chirieac A., Dragoi B., Ungureanu A., Corcodel A.M., Rudolf C., Sasu A., Dumitriu E., (2012), Controlling the activity and chemoselectivity in the cinnamaldehyde hydrogenation by insertion of non-noble metals in the matrix of hydroalcite-like materials, *Environmental Engineering and Management Journal,* **11**, 47-54.

Evans J.W., Wainwright M.S., Bridgewater A.J., Young D.J., (1983), On the determination of copper surface area by reaction with nitrous oxide, *Applied Catalysis,* **7**, 75-83.

Giroir-Fendler A., Richard D., Gallezot P., (1988), *Selectivity in Cinnamaldehyde Hydrogenation of Group-VIII Metals Supported on Graphite and Carbon*, In: *Studies in Surface Science and Catalysis,* Guisnet M., Barbier J., Barrault J., Bouchoule C., Duprez D., Pérot G., Montassier C. (Eds.), Elsevier, 171-178.

Grandsire A.F., Laborde C., Lamaty F., Mehdi A., (2010), Palladium supported on polyether-functionalized mesoporous silica. Synthesis and application as catalyst for Heck coupling reaction, *Applied Organometallic Chemistry,* **24**, 179-183.

Gutiérrez V.S., Diez A.S., Dennehy M., Volpe M.A., (2011), Cu incorporated MCM-48 for the liquid phase hydrogenation of cinnamaldehyde, *Microporous and Mesoporous Materials*, **141**, 207-213.

Gutiérrez V., Alvarez M., Volpe M.A., (2012), Liquid phase selective hydrogenation of cinnamaldehyde over copper supported catalysts, *Applied Catalysis A: General*, **413-414**, 358-365.

Guvelioglu G.H., Ma P., He X., Forrey R.C., Cheng H., (2006), First principles studies on the growth of small Cu clusters and the dissociative chemisorption of H_2, *Physical Review B,* **73**, 155436-1 – 155436-10.

Hájek J., Kumar N., Mäki-Arvela P., Salmi T., Murzin D. Y., Paseka I., Heikkilä T., Laine E., Laukkanen P., Väyrynen J., (2003), Ruthenium-modified MCM-41 mesoporous molecular sieve and Y zeolite catalysts for selective hydrogenation of cinnamaldehyde, *Applied Catalysis A: General,* **251**, 385-396.

Imperor-Clerc M., Bazin D., Appay M.D., Beaunier P., Davidson A., (2004), Crystallization of β-MnO_2 nanowires in the pores of SBA-15 silicas: in situ investigation using synchrotron radiation, *Chemistry of Materials*, **16**, 1813-1821.

Jansat S., Pelzer K., García-Antón J., Raucoules R., Philippot K., Maisonnat A., Chaudret B., Guari Y., Mehdi A., Reyé C., Corriu R.J.P., (2007), Synthesis of new RuO_2@SiO_2 composite nanomaterials and their application as catalytic filters for selective gas detection, *Advanced Functional Materials,* **17**, 3339-3347.

Jun K.-W., Shen W.-J., Rama Rao K.S., Lee K.-W., (1998), Residual sodium effect on the catalytic activity of Cu/ZnO/Al_2O_3 in methanol synthesis from CO_2 hydrogenation, *Applied Catalysis A: General,* **174**, 231-238.

Jung A., Jess A., Schubert T., Schutz W., (2009), Performance of carbon nanomaterial (nanotubes and nanofibres) supported platinum and palladium catalysts for the hydrogenation of cinnamaldehyde and of 1-octyne, *Applied Catalysis A-General,* **362**, 95-105.

Krishna R.G., Rama Rao K.S., Kanta Rao P., (1999), Effect of support modification by carbon coverage in the dehydrogenation activity of Cu/Al_2O_3 catalyst, *Catalysis Letters,* **59**, 157-160.

Kruk M., Jaroniec M., (2001), Gas adsorption characterization of ordered organic−inorganic nanocomposite materials, *Chemistry of Materials,* **13**, 3169-3183.

Li Y., Ge C.H., Zhao J., Zhou R.X., (2008), Influence of preparation modes on Pt-Ni/CNTs catalysts used in the selective hydrogenation of cinnamaldehyde to hydrocinnamaldehyde, *Catalysis Letters,* **126**, 280-285.

Liu H.L., Yuan M.L., Guo C.H., Li R.X., Fu H.Y., Chen H., Li X.J., (2011), Selective hydrogenation of cinnamaldehyde to cinnamyl alcohol over Ru/ZrO2·xH2O catalyst, *Chinese Journal of Catalysis,* **32**, 1256-1261.

Liu C.H., Lai N.C., Lee J.F., Chen C.S., Yang C.M., (2014), SBA-15-supported highly dispersed copper catalysts: Vacuum–thermal preparation and catalytic studies in propylene partial oxidation to acrolein, *Journal of Catalysis*, **316**, 231-239.

López-Linares F., Gonzalez M.G., Páez D.E., (1999), The regioselective biphasic hydrogenation of trans-cinnaldehyde by meta sulfonatophenyl-diphenylphosphine (TPPMS) Ru(II) and Os(II) species. The influence of ionic strength, ligand tensoactivity and metal nature in the selective production of the unsaturated alcohol, *Journal of Molecular Catalysis A: Chemical,* **145**, 61-68.

Mäki-Arvela P., Hájek J., Salmi T., Murzin D.Y., (2005), Chemoselective hydrogenation of carbonyl compounds over heterogeneous catalysts, *Applied Catalysis A: General,* **292**, 1-49.

Morse M.D., Geusic M.E., Heath J.R., Smalley R.E., (1985), Surface reactions of metal clusters. II. Reactivity surveys with D_2, N_2, and CO, *The Journal of Chemical Physics,* **83**, 2293-2304.

Munnik P., Wolters M., Gabrielsson A., Pollington S.D., Headdock G., Bitter J.H., De Jongh P.E. , De Jong K.P., (2011), Copper nitrate redispersion to arrive at highly active silica-supported copper catalysts, *The Journal of Physical Chemistry C,* **115**, 14698-14706.

Reyes P., Rodríguez C., Pecchi G., Fierro J.L.G., (2000), Promoting effect of Mo on the selective hydrogenation of cinnamaldehyde on Rh/SiO_2 catalysts, *Catalysis Letters,* **69**, 27-32.

Richard D., Gallezot P., Neibecker D., Tkatchenko I., (1989), Characterization and selectivity in cinnamaldehyde hydrogenation of graphite-supported platinum catalysts prepared from a zero-valent platinum complex, *Catalysis Today,* **6**, 171-179.

Rylander P.N., (1967), *14 - Hydrogenation of Aldehydes*, *In: Catalytic Hydrogenation over Platinum Metals,* Rylander P.N. (Ed.), New York, USA: Academic Press, 238-256.

Samant P.V., Pereira M.F.R., Figueiredo J.L., (2005), Mesoporous carbon supported Pt and Pt-Sn catalysts for hydrogenation of cinnamaldehyde, *Catalysis Today,* **102**, 183-188.

Sietsma J.R.A., Meeldijk J.D., Versluijs-Helder M., Broersma A., van Dillen A.J., de Jongh P.E., de Jong, K.P., (2008), Ordered mesoporous silica to study the preparation of Ni/SiO_2 ex nitrate catalysts: impregnation, drying, and thermal treatments, *Chemistry of Materials*, **20**, 2921–2931.

Tian W.H., Sun L.B., Song X.L., Liu X.Q., Yin Y., He G.S., (2010), Adsorptive desulfurization by copper species within confined space, *Langmuir*, **26**, 17398-17404.

Toebes M.L., Prinsloo F.F., Bitter J.H., Van Dillen A.J., De Jong K.P., (2003), Influence of oxygen-containing surface groups on the activity and selectivity of carbon nanofiber-supported ruthenium catalysts in the hydrogenation of cinnamaldehyde, *Journal of Catalysis,* **214**, 78-87.

Toupance T., Kermarec M., Louis C., (2000), Metal particle size in silica-supported copper catalysts. influence of the conditions of preparation and of thermal pretreatments, *Journal of Physical Chemistry B,* **104**, 965-972.

Tu C.-H., Wang A.-Q., Zheng M.-Y., Wang X.-D., Zhang T., (2006), Factors influencing the catalytic activity of SBA-15-supported copper nanoparticles in CO oxidation, *Applied Catalysis A: General*, **297**, 40-47.

Ungureanu A., Dragoi B., Chirieac A., Ciotonea C., Royer S., Duprez D., Mamede A.S., Dumitriu E., (2013), Composition-dependent morphostructural properties of Ni-Cu oxide nanoparticles confined within the channels of ordered mesoporous SBA-15 silica, *ACS Applied Materials and Interfaces,* **5**, 3010-3025.

Yang Y., Evans J., Rodriguez J.A., White M.G., Liu P., (2010), Fundamental studies of methanol synthesis from CO_2 hydrogenation on Cu(111), Cu clusters, and Cu/ZnO(0001), *Physical Chemistry Chemical Physics,* **12**, 9909-9917.

Yin Y., Xue D. M., Liu X.Q., Xu G., Ye P., Wu M.Y., Sun L.B., (2012), Unusual ceria dispersion formed in confined space: a stable and reusable adsorbent for aromatic sulfur capture, *Chemical Communications*, **48**, 9495-9497.

Yuan Q., Yin A.-X., Luo C., Sun L.-D., Zhang Y.-W., Duan W.-T., Liu H.-C., Yan C.-H., (2008), Facile synthesis for ordered mesoporous γ-aluminas with high thermal stability, *Journal of the American Chemical Society,* **130,** 3465-3472.

Zheng X.-C., Wu S.-H., Wang S.-P., Wang S.-R., Zhang S.-M., Huang W.-P., (2005), The preparation and catalytic behavior of copper–cerium oxide catalysts for low-temperature carbon monoxide oxidation, *Applied Catalysis A: General*, **283**, 217-223.